17th World Conference on Earthquake Engineering, 17WCEE
Sendai, Japan - September 13th to 18th 2020

EFFECTS OF SLAB AT AN END SPAN IN REINFORCED CONCRETE FRAMES

Ziling.Xiao [1], Toshikazu.Kabeyasawa [2], Toshimi.Kabeyasawa [3]

[1] *Graduate Student, Tokyo Metropolitan University, xiaoziling_syousurin@yahoo.co.jp*
[2] *Associate Professor, Tokyo Metropolitan University, tosikazu0911@gmail.com*
[3] *Professor Emeritus, The University of Tokyo, kabe@eri.u-tokyo.ac.jp*

Abstract

The effective slab width is conventionally taken as 1.0m in the calculation of moment strength of T-shape beams based on the manuals for technical standards in Japanese seismic design code of practice. However, a series of static and seismic loading tests of reinforced concrete frame assemblies representing the interior span conducted from 2010 to 2014, have verified that the whole slab could be fully effective to the flexural strength of beam at around the inter-story drift angle of 1/100rad.

In order to study the effects of slab at the end span, tests on 2/5-scale 1×1 span three-dimensional reinforced concrete frame were conducted at the structural laboratory of Tokyo Metropolitan University in 2017 and 2018 by varying the size of the transverse beams. Four columns were put on the pin roller supports which allowed the axial elongation of beams. The specimen reached the design strength with the full slab section at the drift angle of 2/100 or 3/100 indicating that the evaluation of the effective slab width should be different in continuous span and end span. This is because of the flexural and torsional deformations of the transverse beams. This paper reports on the experimental and analytical study on the 2017 and 2018 tests and the effective slab width of T-shape beams at the end span in seismic design considering rigidity of transverse beams.

In the first test of 2017, the beam sizes of the longitudinal and transverse beams were adopted as relatively weak rigidity with the width of 200mm and the depth of 240mm. The yielding of slab upper rebars was observed at the drift angel of 1/100, and the yielding of the lower rebars at the drift angle of 1/75. Even at the drift of 1/30, some of the slab rebars remained in elastic range. The effective slab width defined with the strain ratios of all rebars to the yield level remained as 0.6 at 1/100, 0.8 at 1/50 and 0.88 even at the maximum deformation angle of 1/30. These ratios could be identified by simple formula based on the idealized nonlinear deformations of the transverse beams.

In the second test of 2018, the width of the beams was changed into 300mm from 200mm of the 2017 specimen. The specimen reached the strength of whole slab at 1/50, which was apparently smaller than that of the 2017 specimen owing to the stiffer transverse beams. The yielding of the slab upper rebar was observed at the drift angle of 0.66/100, and the yielding of the lower rebar was observed at 1/100. Most of the slab upper rebar fully yielded at 1/50, while the lower rebar yielded mostly at 1/30.

The test results showed a relation between the deformation of transverse beam and the strain of slab rebars, while a method to evaluate the drift when full slab is effective at end span is presented which is compared with the relation from the test. The drift calculated by the method is higher than that in test because the influence of the compression side is not considered. The method need be improved further.

Keywords: Effective width of slab, transverse beam, out-of-plane deformation, end span

1. Introduction

The effective slab width is conventionally taken as 1.0m in the calculation of moment strength of T-shape beams based on the manuals for technical standards in Japanese seismic design code. Only the upper slab reinforcing bars are taken into account for the evaluation of moment strength of T-shape beam while the lower have been neglected because the anchorage length is not enough in normal construction details. The underestimation of the moment strength of T-shape beam is allowable in the point of the view from the evaluation of lateral load carrying capacity. However, it might cause the story collapse mechanism in the moment resisting frames, even if the beam-yielding mechanism is assumed in the seismic design.

A series of static and seismic loading tests of reinforced concrete frame assemblies were conducted to identify the effects of slab on the beam strength in 2010, 2012, 2013 and 2014 [1-3]. All of the seven specimens contained continuous span (Fig.1) and the slab reinforcing bars were fully effective to the flexural strength of beams at 1%～1.33% story drift. In above test results, the strain of slab reinforcing bars tended to become smaller gradually as the rebar locates away from the beam side surface. Due to the tensile force of the slab reinforcing bars, particularly at the span end, out-of-plane deformation may occur in the transverse beam that would break the Bernoulli hypothesis and the decrease of slab reinforcing bars strain (Fig.2). Therefore, the stiffness of transverse beam may affect the effective slab width. In order to identify the effect of transverse beam, two tests with different beam section (different rigidity) have been conducted in 2017 and 2018.

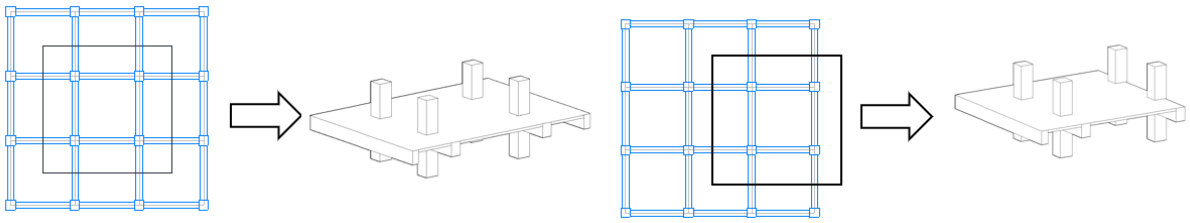

Fig. 1 – Modeling concept of past test specimens

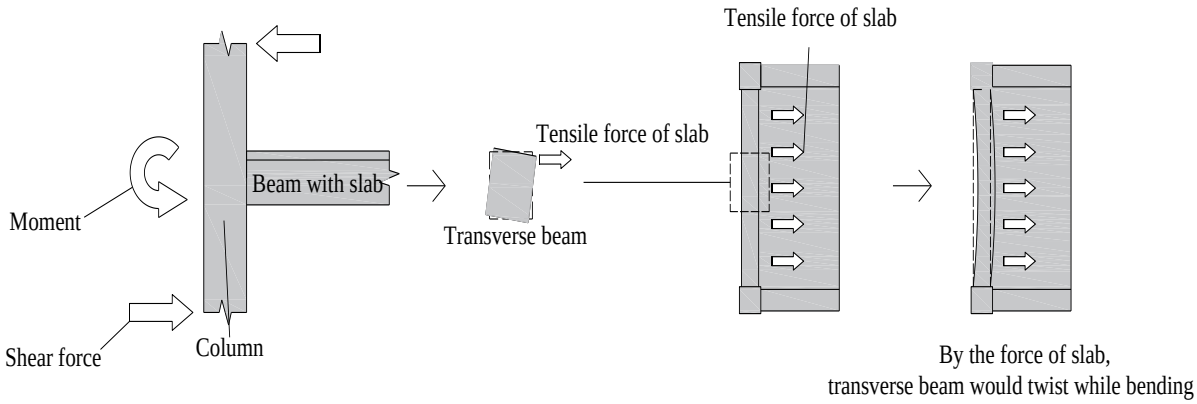

Fig. 2 – Effect of transverse beam

2. Test Plan

2.1 Test Specimens

The 2017 and 2018 specimens are two-fifth scale three-dimensional reinforced concrete moment resisting frame assemblies which idealize the boundary condition of the span end in the middle story of proto-type buildings. The frame consists of a floor slab, four columns, two longitudinal beams and two transverse beams

as shown in Fig.3. All of the columns are supported by pin roller at the bottom. The total height of specimens is 1500mm and the section ends of column are 750mm distant from the center axis of the beams in upper and lower story. The span length is 2500mm in longitudinal and transverse direction. The section of columns is 300 mm square. The width and depth of beams are 200mm and 240mm in 2017 test. Those are 300mm and 240mm in 2018 test. The thickness of slabs is 80mm.

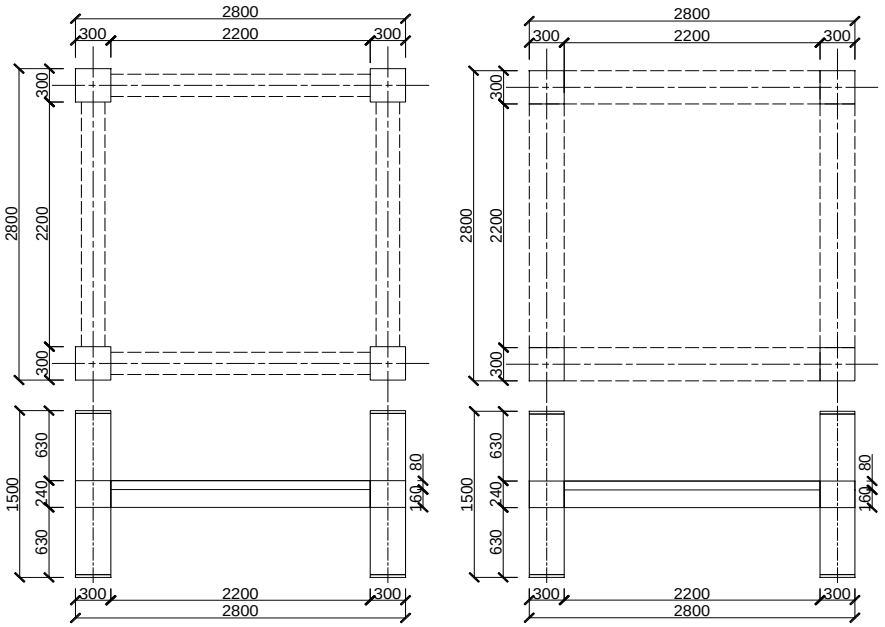

(a) Specimen 2017 (b) Specimen 2018

Fig. 3 – Geometry of specimens (unit: mm)

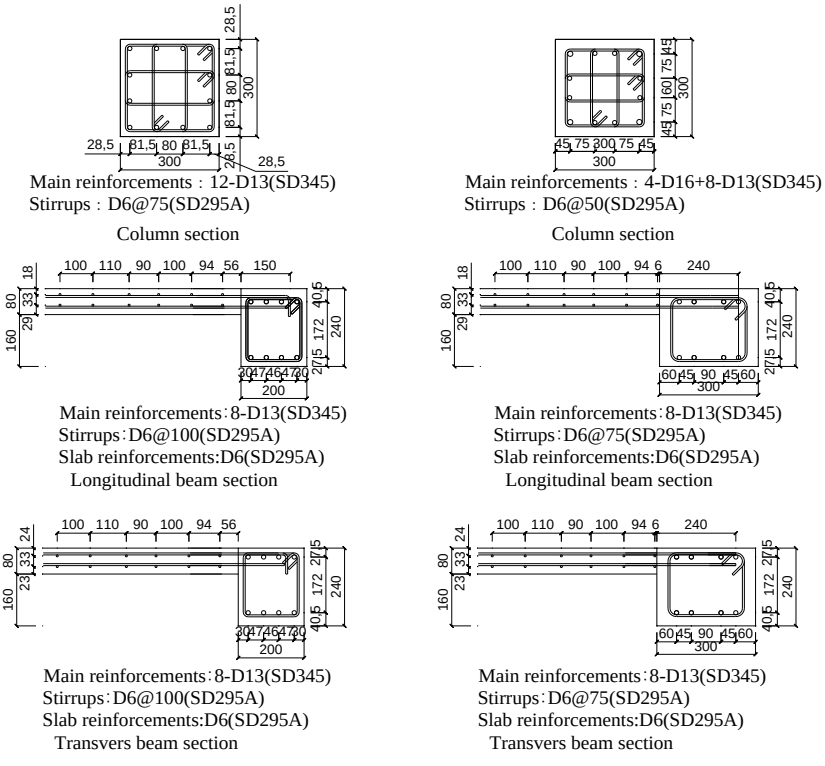

(a) Specimen 2017 (b) Specimen 2018

Fig. 4 – Column and beam sections

The sections of the members are shown in Fig.4. As for the specimen tested in 2017, the columns have 12-D13(SD345) rebar as main reinforcements and 4-D6 (SD295) rebar with 75 mm spacing as hoops and sub-hoops. The beams have 4-D13(SD345) rebar as either of top or bottom reinforcement. The beams also have 2-D6(SD295) rebar with 100mm spacing as stirrups. And the reinforcement of slab was D6(SD295) rebar double with 100mm spacing in both longitudinal and transverse direction. The reinforcement of specimen tested in 2018 was almost the same with the specimen tested in 2017 except for the section of columns and the spacing of stirrup. Reinforcements at four corners in the column section replace D16(SD345) rebar. The spacing of the stirrup is changed to 75mm.

The results of the material tests are shown in Table 1. and Table 2. Due to the difference of the season for the static loading tests, the strength of concrete is slightly different in the two tests.

Table 1 – Material properties of concrete(N/mm^2)

	Compressive strength	Elastic Modulus
2017	33.4	27.6×10^3
2018	28.4	26.1×10^3

Table 2 – Material properties of reinforcing steel

Steel bars	Yield strength (N/mm^2)	Peak strength (N/mm^2)	Yield strain (μ)
D13(SD345)	363	550.6	1924
D6(SD295)	360.5	516.8	1995

2.2 Loading Method

A schematic of the loading setup is shown in Fig.5. In order to release the axial forces on beam sections caused by their elongation, four columns were put on the pin roller supports. Specimens are fixed in the vertical direction by the pretension of PC steel bar attached to the base frame and the column top through the center hole in the column section. It prevents the uplift of the column base by the shear force of beams. A 75kN axial force is induced to each column. The steel girder is fixed to the side surface of two columns parallel to the transverse beams. Four girders are totally attached in upper and lower story on east and west side. Four loading jacks were attached to the center of each steel girders, and the other side of jacks are attached either to the reaction wall or the reaction frame. The static cyclic loading tests are carried out with increasing the peak story drift from 0.25% to 3.33%. The drifts of the four columns are made to be identical in the test, by controlling the lateral loading jacks on the east and west sides manually.

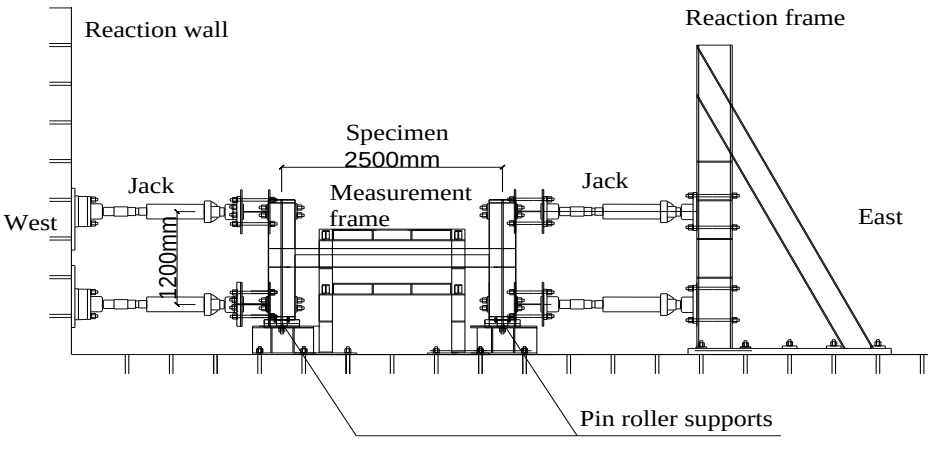

Fig. 5 – Loading set up

3. Results of Tests

3.1 Observed response

The global hysteretic relations of story shear force and drift ratio are shown in Fig.6. The calculation of lateral load carrying capacity is shown by dashed line for a conventional model with 400mm cooperated width of slab in T-shape beam section (the width considered to be 2/5 scale) and by solid line for a model with fully cooperated width of slab. In the case of 2017 test, observed strengths in the negative direction are significantly lower, possibly due to incorrect operations. In the positive direction, the specimen in 2017 test reached the design strength with the conventional slab section at 0.5% drift and the design strength with the full slab section at 2%~3.33% drift. Because of the improvement of operation, the strength in negative direction of specimen in 2018 test was not much different from the positive direction. The specimen in 2018 test reached the design strength with the conventional slab section at 0.5% and the design strength with the full slab section at 2% in both directions. The result was different from the past tests results on assembled frame with the continuous span, in which the strength of the specimen exceeded the design strength with the full slab section at 1%~1.33% drift. The moment strength of T-shape beam section is evaluated by:

$$M_y=0.9a_b\sigma_{by}d+0.9a_s\sigma_{sy}d_s \quad (1)$$

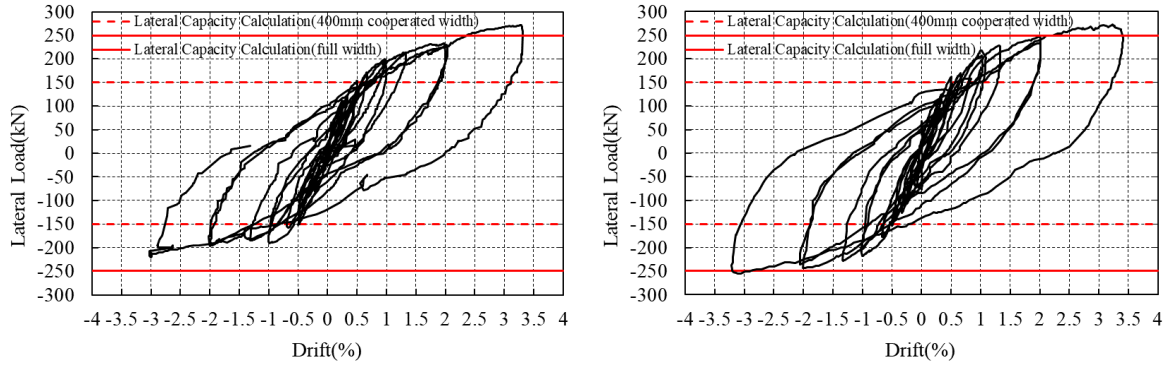

(a) Specimen 2017 (b) Specimen 2018

Fig. 6 – Loading displacement relations

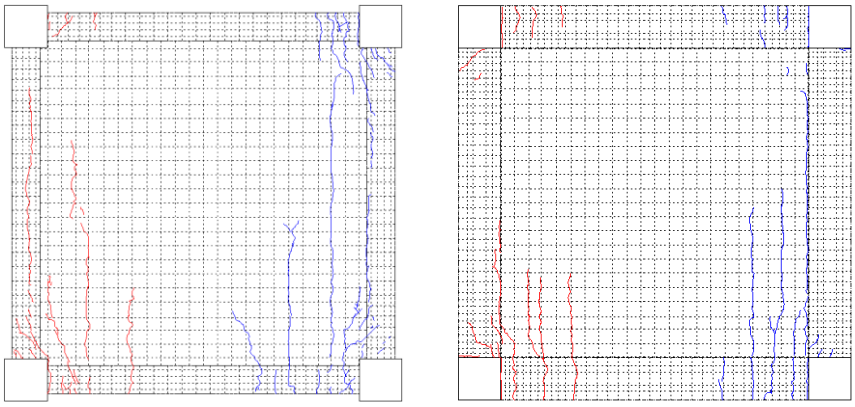

(a) Specimen 2017 (b) Specimen 2018

Fig. 7 – Cracks on slab observed at the drift of 1%

3.2 Measured strain and deformation

The tensile stress on slab reinforcing rebar at the face of transverse beam is evaluated from the stress strain relation in the material test results. The test results are shown in Fig. 8. The stress was reduced as rebar locates away from the beam column joint in transverse direction. In the 2017 test, the yielding of upper rebar is

confirmed at 1% drift, and the yielding of the lower rebar is confirmed at 1.33% drift. At 3.33% drift, not all of the rebars have yielded. In 2018 test, the yielding of upper rebar is confirmed at 0.66% drift, and the yielding of the lower rebar is confirmed at 1% drift. The upper rebar almost completely yielded at 2% drift, and the lower rebar yielded at 3.3% drift. Apparently, the stress of the slab reinforcing rebar is significantly higher in 2018 test rather than in 2017 test.

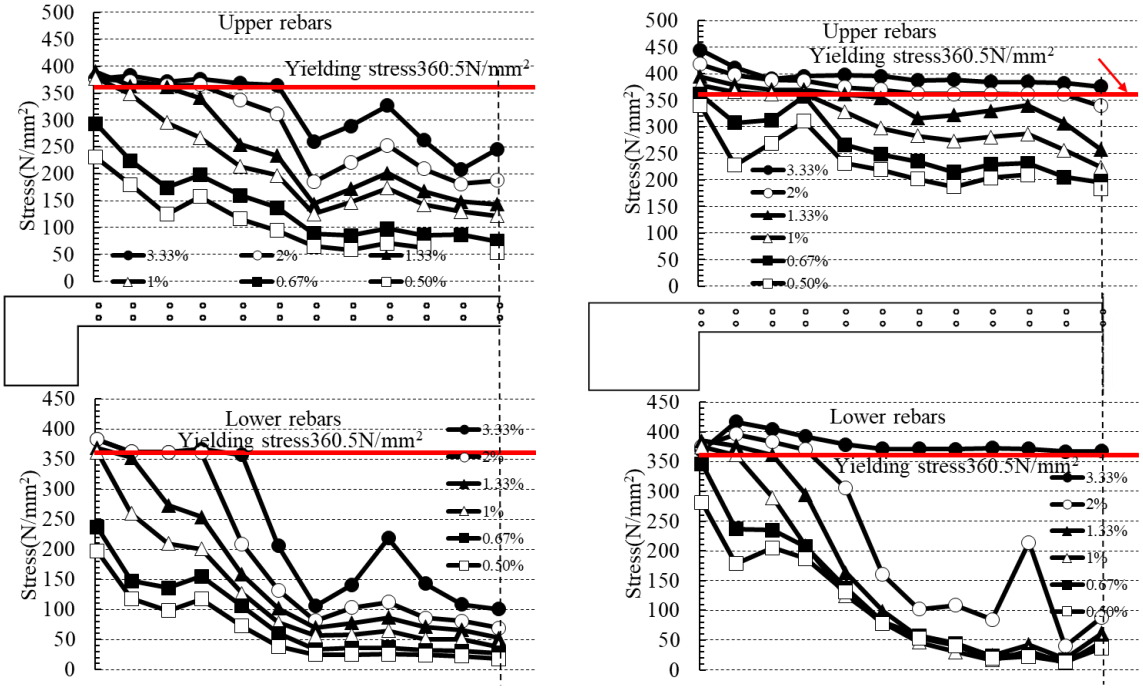

(a) Specimen 2017 (b) Specimen 2018

Fig. 8 – Stress of slab rebar

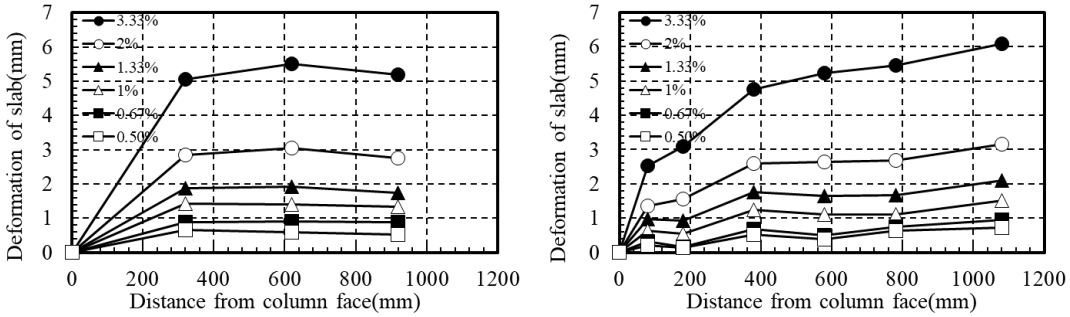

(a) Specimen 2017 (b) Specimen 2018

Fig. 9 – Deformation of slab

The deformation of the transverse beam contains out of plane bending deformation and torsional deformation due to the tensile force by the slab reinforcement. In the test, the horizontal displacement of the transverse beam in the loading direction is measured. It is measured at the height of top and bottom of the transverse beams and several measuring points are distributed in the transverse direction. The horizontal deformation at the height of the slab center axis is obtained from the records, and relative displacement from the end of longitudinal beam is shown in Fig.9. The relative deformation of the transverse beams in 2017 test is slightly higher than that in 2018 test. Due to the higher rigidity of transverse beam, though the stress of slab reinforcing bars was higher, the relative deformation is smaller in 2018 test.

3.3 Relations between the transverse beam deformation and the slab rebar strain

In order to get the drift when the whole slab is fully effective analytically, a theoretical method is developed. In the process of derivation, a difficult problem is how to confirm the stress distribution in the slab rebars. Based on the deformation compatibility condition on boundary, it can be simply judged that the strain distribution is related to the deformation of the transverse beam. The relation between the difference of tensile strains and the difference of the slab deformation considering transverse beam's torsional and bending deformation of two slab rebars at different position in transverse direction is shown in Fig.10. The initial deformation difference is not zero because of a measurement error. It can be divided into three stage. At 1st and 3rd stage, they are approximately linearly correlation and the slope based on the final point of 1st stage is increasing at 2nd stage. It can be considered that the transition from 1st stage to 2nd stage is due to the form of tension shift in rebar with larger strain and the transition from 2nd stage to 3rd stage is due to the form of tension shift in the rebar with lower strain.

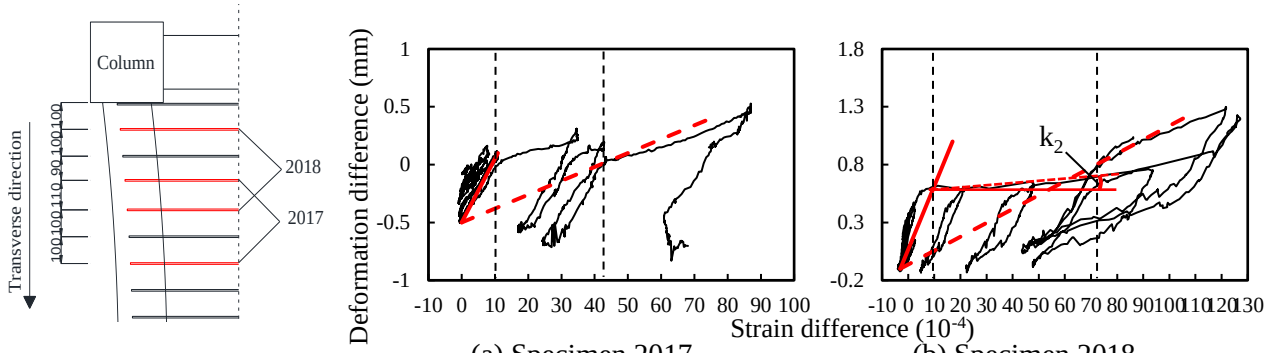

(a) Specimen 2017 (b) Specimen 2018

Fig. 10 – Relation between deformation difference and strain difference

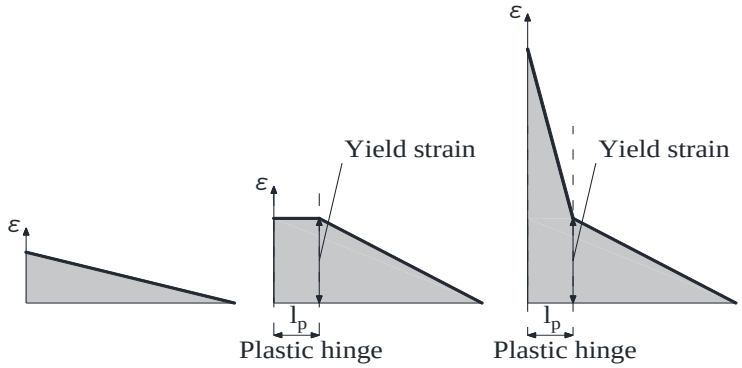

Fig. 11 – Strain progression

The relation can also be derived theoretically. Reference to Guidelines for Performance Evaluation of Earthquake Resistant Reinforced Concrete Buildings (Draft) [4], the strain distribution of reinforcement bar can be assumed as Fig.11. And in this paper, the length of plastic hinge is assumed as D, which is the depth of beam. Before two rebars have yielded, the relation is

$$\delta_2-\delta_1=\frac{1}{2}(\varepsilon_1-\varepsilon_2)\frac{L}{2} \tag{2}$$

As shown in Fig.10, the initial slope of tests is almost L/4 same. Because of tension shift, when the rebar with larger strain is close to yield, its strain distribution will no longer be a triangle distribution. However, strain in plastic hinge would increase and the strain distribution will change into a triangle distribution at a

certain time just as shown in Fig.12. So, when $\varepsilon<\varepsilon_y'=\varepsilon_y/(1-2l_p/L)$, although the ratio of two differences would fluctuate slightly, it can still be assumed that the Eq. (2) is tenable.

Then with the increasement of strain in plastic hinge, the relation is

$$\delta_2-\delta_1=\frac{1}{2}(\varepsilon_1-\varepsilon_y')l_p+\frac{1}{2}(\varepsilon_y'-\varepsilon_2)\frac{L}{2} \tag{3}$$

For the end point of the previous stage, the slope is

$$k_2=\frac{\Delta\delta-\Delta\delta_y}{(\varepsilon_1-\varepsilon_2)-(\varepsilon_y'-\varepsilon_2^y)}=\frac{\frac{1}{2}(\varepsilon_1-\varepsilon_y')l_p+\frac{1}{2}(\varepsilon_y'-\varepsilon_2)\frac{L}{2}-\frac{1}{2}(\varepsilon_y'-\varepsilon_2^y)\frac{L}{2}}{(\varepsilon_1-\varepsilon_2)-(\varepsilon_y'-\varepsilon_2^y)} \tag{4}$$

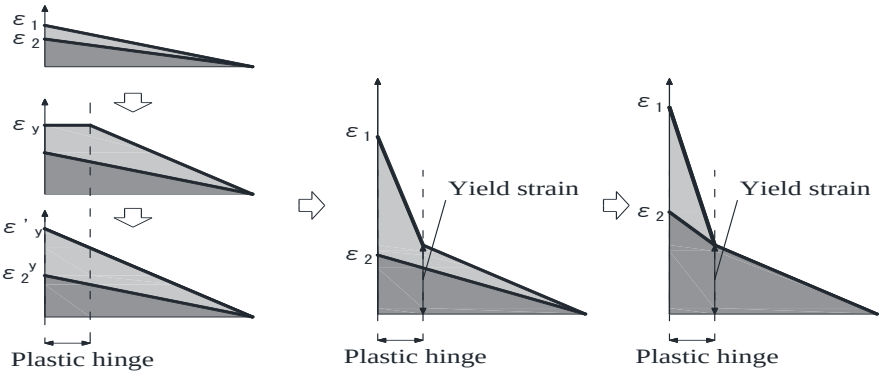

Fig. 12 – Strain progression of two different rebars

Rearranging Eq. (4) yields the following equation

$$k_2=\frac{L}{4}-\alpha\left(\frac{L}{4}-\frac{l_p}{2}\right) \tag{5}$$

where

$$\alpha=\frac{\varepsilon_1-\varepsilon_y'}{(\varepsilon_1-\varepsilon_y')-(\varepsilon_2-\varepsilon_2^y)} \tag{6}$$

k_2 in tests is about 50mm initially, and α is 1.163 when k_2 is substituted in Eq. (6). Although α is related with the increasing rate of two rebars' strain and would change with the position of two rebars, there is a possibility that it would be 1.163 that shows that the theoretical and tests results are in agreement.

When the rebar with small strain yields, the relation between two differences would be

$$\delta_2-\delta_1=\frac{1}{2}(\varepsilon_1-\varepsilon_2)l_p \tag{7}$$

The secant stiffness at this stage is D/2 = 120mm, which is almost consistent with Fig.10.

Thus, the deformation-strain difference relation between theory and experiment is approximately consistent. However, in the frame with slab, the strength of the slab tension side and the compression side is different, so the inflection point is not at the center. The position would not change so much, and for the convenience of calculation, the center position of the beam is treated as the inflection point.

4. Method to evaluate the drift when full slab is effective at end span

At the drift when the strength of specimens reached the design strength in the model with full slab section, not all slab reinforcing bars have yielded for either specimen. It assumes that a part of beam main bars and slab reinforcing bars exceeds the nominal yielding stress due to the strain hardening effect, and it complemented the unyielding stress of slab reinforcing bars in the middle span.

$$\sum a_b f_{bi} j_i + \sum a_s f_{si} j_i = \sum a_b f_{yb} j_i + \sum a_s f_{ys} j_i \tag{8}$$

Based on the relation between slab rebars' strain and the deformation of transverse beam, If the yield point is taken as the basic point, the strain of slab rebar at arbitrary position is

$$\varepsilon(x) = \frac{\delta_y}{l_r} - \frac{\delta(x)}{l_r} + \frac{f_{ys}}{E_s} \tag{9}$$

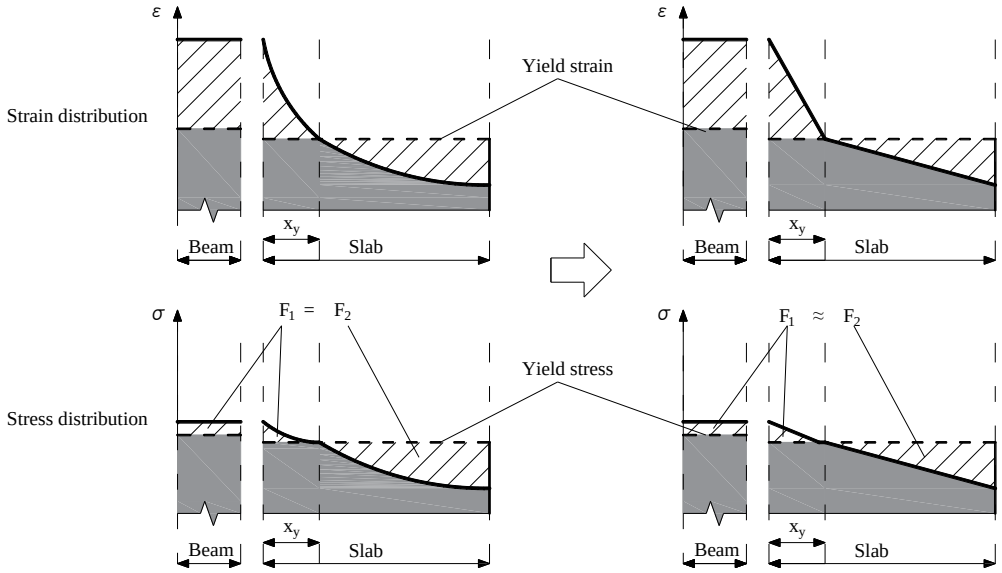

Fig. 13 – Strain and stress distribution in transverse direction

If calculating the strain of rebars at each position and adding them up, it's difficult to formulate for arbitrary case. So as shown in Fig.13, it can be considered as distributed load for integration.

Substitution of Eq. (9) in Eq. (8) gives

$$n_s \rho_{ts} D_s E_s' \int_0^{x_y} \left(\frac{\delta_y}{D/2} - \frac{\delta(x)}{D/2} - (\gamma_s - 1) \frac{f_{ys}}{E_s} \right) dx + E_{sb}' a_b \left(\frac{\delta_y}{D/2} + \frac{f_{ys}}{E_s} - \gamma_b \frac{f_{yb}}{E_{sb}} \right) = n_s \rho_{ts} D_s E_s \int_{x_y}^{\frac{L_t}{2}} \left(\frac{\delta(x)}{L/4} - \frac{\delta_y}{L/4} \right) dx \tag{10}$$

Where j_i is assumed to be the same. For the deformation, assuming that all the slab rebars have yielded, considering stiffness degradation of torsional deformation and bending deformation, it can be given by

$$\delta(x) = \frac{\rho_{ts} D_s f_{ys}}{\alpha_b(x) EI} \left(\frac{L_t^2}{24} x^2 - \frac{L_t}{12} x^3 + \frac{1}{24} x^4 \right) + \frac{\rho_{ts} D_s f_{ys} (D - D_s)^2 x (L_t - x)}{\alpha_t(x) 8GJ} \tag{11}$$

However, since the fourth power of x_y is included in the equation, it is difficult to integrate and solve from Eq. (10). Therefore, the deformation distribution is simplified as linear distribution shown in Fig.13:

$$\delta(x)=\left(\frac{\rho_{ts}D_s f_{ys}L_t^4}{384EI}+\frac{\rho_{ts}D_s f_{ys}(D-D_s)^2L_t^2}{32GJ}\right)\frac{x}{L_t/2}=(\delta_b+\delta_t)\frac{2x}{L_t} \tag{12}$$

Assuming stiffness degradation forms only from end to yield point. Substitution of Eq. (12) in Eq. (10) gives:

$$\begin{aligned}&\left(\frac{\delta_b}{\alpha_b}+\frac{\delta_t}{\alpha_t}\right)n_s\rho_{ts}D_sE_s'\frac{2}{DL_t}\left[x_y-\frac{(\gamma_s-1)\frac{f_{ys}}{E_s}}{\left(\frac{\delta_b}{\alpha_b}+\frac{\delta_t}{\alpha_t}\right)\frac{4}{DL_t}}\right]^2+E_{sb}'a_b\left[\left(\frac{\delta_b}{\alpha_b}+\frac{\delta_t}{\alpha_t}\right)\frac{4x_y}{DL_t}+\frac{f_{ys}}{E_s}-\gamma_b\frac{f_{yb}}{E_{sb}}\right]\\&=\frac{4(\delta_1+\delta_2)n_s\rho_{ts}D_sE_s}{L}\left(\frac{L_t}{4}+\frac{x_y^2}{L_t}-x_y\right)\end{aligned} \tag{13}$$

When calculating the deformation, it was assumed that all rebars have yielded, but rebars at center did not actually yield. Moreover, bending moment at the end is greatly affected by the load at center. It is necessary to reduce the bending deformation δ_b.

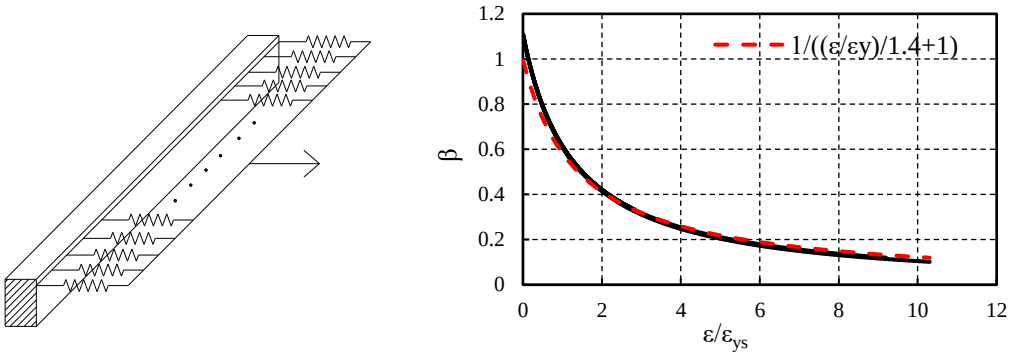

Fig. 14 – Elastic model of transverse beam and reduction coefficient of bending deformation

In order to obtain the reduction coefficient, an elastic model shown in Fig.14 is established. Springs are used to simulate rebars and the length of springs is L/4. Loading all spring the displacement of $L/4\times1.1\varepsilon_{ys}$ to simulate the stress distribution in the actual situation. For arbitrary section, the diagram shown in Fig.13 can be earned where

$$\beta=\delta_{mid}/\frac{\rho_{ts}D_s f_{ys}L_t^4}{384EI} \tag{14}$$

$$\varepsilon/\varepsilon_{ys}=\left(\frac{\rho_{ts}D_s f_{ys}L_t^4}{384EI}+\frac{\rho_{ts}D_s f_{ys}(D-D_s)^2L_t^2}{32GJ}\right)/\frac{L\varepsilon_{ys}}{4} \tag{15}$$

The curve could be represented by

$$\beta=\frac{1}{(\varepsilon/\varepsilon_{ys})/1.4+1} \tag{16}$$

Regarding the stiffness degradation rate, the bending stiffness degradation rate a_b is calculated by Sugano's equation (Eq. (17)). There are few studies about torsional stiffness degradation, especially about bending torsion, so it's difficult to use a method calculating the torsional stiffness degradation rate. Since the ratio of torsional deformation is comparatively low, the torsional stiffness degradation rate a_t is simply set as 0.228.

$$\alpha_y=(0.043+1.64n\rho_t+0.043a/D)(d/D)^2 \tag{17}$$

Rearranging equation (9) gives a quadratic equation for x_y

$$\left[\frac{4(\beta\delta_b+\delta_t)n_s\rho_{ts}D_sE_s}{LL_t}-\left(\frac{\beta\delta_b}{\alpha_b}+\frac{\delta_t}{\alpha_t}\right)\frac{2n_s\rho_{ts}D_sE_s'}{DL_t}\right]x_y^2$$
$$-\left[\frac{4(\beta\delta_b+\delta_t)n_s\rho_{ts}D_sE_s}{L}+\left(\frac{\beta\delta_b}{\alpha_b}+\frac{\delta_t}{\alpha_t}\right)\frac{4E_{sb}'a_b}{DL_t}-n_s\rho_{ts}D_sE_s'(\gamma_s-1)\frac{f_{ys}}{E_s}\right]x_y \tag{18}$$
$$+\frac{(\beta\delta_b+\delta_t)n_s\rho_{ts}D_sE_sL_t}{L}+E_{sb}'a_b(\gamma_b\frac{f_{yb}}{E_{sb}}-\frac{f_{ys}}{E_s})-\frac{n_s\rho_{ts}D_sE_s'DL_t((\gamma_s-1)\frac{f_{ys}}{E_s})^2}{8\left(\frac{\beta\delta_b}{\alpha_b}+\frac{\delta_t}{\alpha_t}\right)}=0$$

If x_y is known, the strain of the beam rebar can be calculated from Eq. (9).

$$\varepsilon_b=\left(\frac{\beta\delta_b}{\alpha_b}+\frac{\delta_t}{\alpha_t}\right)\frac{4x_y}{DL_t}+\frac{f_{ys}}{E_s} \tag{19}$$

The plastic hinge rotation R_p is given by

$$R_p=\frac{(\varepsilon_b-f_{yb}/E_{sb})D}{2d_n} \tag{20}$$

The yield rotation angle R_y is calculated by

$$R_y=\frac{M_yL}{\alpha_y6EI} \tag{21}$$

Where M_y is moment strength with full slab section and α_y is stiffness degradation rate. α_y is calculated by Sugano's equation (Eq. (17)), but it should be attention that the reinforcement ratio needs to consider the reinforcement bars of slab. Referring to previous research [5], rebars of slab within 0.1L from the edge of beam is considered.

The drift when the full slab is effective is the sum of the two:

$$R_f=R_p+R_y \tag{22}$$

The drifts are calculated for the test specimens and compared with the test results as shown in Table 3. The calculated drifts are larger than those of the test results, which may still conservative from the viewpoint of the beam strength evaluation, which may be adopted for design practice. One of the reasons might be because the influence of compression side is not considered in the calculation. The method need be improved further.

Table 3 – Comparison of test results and calculation results

Drift when full slab is effective(rad)	2017	2018
Test	0.024	0.020
Calculation	0.034	0.023

5. Conclusions

This paper shows the test results on three-dimensional moment resisting frames with the floor slab representing the span end of the building in order to evaluate the effective slab width of the T-shape beam section. The numerical analyses are also carried out for simulating the test results. The following conclusions are obtained:

1) The lateral load carrying capacity of two specimens reached the strength in calculation with a model assumed the conventional slab width in T-shape beam section at 0.5% drift and the strength in calculation with a model assumed full slab section at 2% to 3.3% drift. This result is different from the past test results on the moment resisting frame which contains the continuous span, which reached the strength calculated with the full slab width at 1% ~1.33% drift. The test results indicate that the methods for evaluating the effective slab width in relation to the drift level should be different between the inner continuous span and the end span considering the rigidity and the deformation of the transverse beam.

2) Load-displacement relationships, the tensile strains in the slab reinforcing rebars and the deformation of the transverse beams are different between the two specimens, where only the widths of the beam section are varied. The tensile strains in the slab reinforcing rebars are relatively larger in the 2018 test owing to the higher rigidity of the transverse beams.

3) An analytical method is presented to evaluate the drift when the full slab section is to be effective. The calculation drifts are higher than those of the test results probably because the influence of compression side is not considered. The method need be improved further.

6. Notations

a : Shear span which is taken as 0.2L at transverse beam and 0.5L at longitudinal beam; a_b : Area of beam rebar; a_s : Area of slab rebar; d : Distance from beam tensile rebar to compression side edge; d_s : Distance from slab tensile rebar to compression side edge; d_n : Distance from tensile rebar to neutral axis; D : Beam section depth; D_s : Slab depth; f_{bi} : Stress of beam rebar; E : Concrete elastic modulus; E_s : Elastic modulus of slab rebar; E_{sb} : Elastic modulus of beam rebar; E_s' : Hardening modulus of slab rebar; E_{sb}' : Hardening modulus of beam rebar; f_{si} : Stress of slab rebar; f_{yb} : yield stress of beam rebar; f_{ys} : yield stress of slab rebar; I : Moment of inertia of area; j_i : Distance between tensile force and compressive force; l_r : $\Delta\delta/\Delta\varepsilon$; L : Longitudinal beam length; L_t : Transverse beam length; n : Ratio steel elastic modulus to concrete elastic modulus; n_s : number of slab's side; α_b : Bending stiffness degradation rate; α_t : Torsional stiffness degradation rate; γ_s : Ratio of strain at first hardening to yield strain of slab rebar; γ_b : Ratio of strain at first hardening to yield strain of beam rebar; δ_y : Deformation of yield point in transverse direction; ρ_{ts} : slab reinforcement ratio; ρ_t : Beam tensile reinforcement ratio;

7. References

[1] Xuan Deng, Toshikazu Kabeyasawa, Toshimi Kabeyasawa, Hiroshi Fukuyama (2012): Experimental study on a three-dimensional RC frame with slab subjected to lateral loads. *Japan Concrete Institute*, 331-336.

[2] Kim Geol, Kabeyasawa Toshikazu, Kabeyasawa Toshimi, Fukuyama Hiroshi (2016): A Study on Effective Width of Slab on Reinforced Concrete Beam in Assembled Frame Specimens (Part 6) Simulation by FEM Analysis(*in Japanese*). *Annual Convention*, AIJ, Vol. ST-III, No. 23139, 257-258.

[3] Kabeyasawa Toshimi, Kabeyasawa, Toshikazu (2017): Effective Slab Width for Evaluating Ultimate Seismic Capacities of Reinforced Concrete Buildings. *Proceedings of the 4th Congrès International de Géotechnique-Ouvrages-Structures, Congrès International de Géotechnique-Ouvrages-Structures*, 15-29.

[4] *Guidelines for Performance Evaluation of Earthquake Resistant Reinforced Concrete Buildings (Draft)*, AIJ.

[5] LEE Sangho, Tasai Akira, Kotani Shunsuke, Aoyama Hiroyuki (1990): Flexural strength and yield point rigidity of reinforced concrete T-beams, *AIJ Annual Convention*, 303-304.

